Variability of Aerosol Optical Properties at Four North American Surface Monitoring Sites

DAVID J. DELENE

CIRES, University of Colorado, Boulder, and NOAA, Boulder, Colorado

JOHN A. OGREN

NOAA Climate Monitoring and Diagnostics Laboratory, Boulder, Colorado

(Manuscript received 27 February 2001, in final form 15 August 2001)

ABSTRACT

Aerosol optical properties measured over several years at surface monitoring stations located at Bondville, Illinois (BND); Lamont, Oklahoma (SGP); Sable Island, Nova Scotia (WSA); and Barrow, Alaska (BRW), have been analyzed to determine the importance of the variability in aerosol optical properties to direct aerosol radiative forcing calculations. The amount of aerosol present is of primary importance and the aerosol optical properties are of secondary importance to direct aerosol radiative forcing calculations. The mean aerosol light absorption coefficient (σ_{ap}) is 10 times larger and the mean aerosol scattering coefficient (σ_{sp}) is 5 times larger at the anthropogenically influenced site at BND than at BRW. The aerosol optical properties of single scattering albedo (ω_o) and hemispheric backscatter fraction (b) have variability of approximately $\pm 3\%$ and $\pm 8\%$, respectively, in mean values among the four stations. To assess the importance of the variability in ω_o and b on top of the atmosphere aerosol radiative forcing calculations, the aerosol radiative forcing efficiency ($\Delta F/\delta$) is calculated. The $\Delta F/\delta$ is defined as the aerosol forcing (ΔF) per unit optical depth (δ) and does not depend explicitly on the amount of aerosol present. Based on measurements at four North American stations, radiative transfer calculations that assume fixed aerosol properties can have errors of 1%–6% in the annual average forcing at the top of the atmosphere due to variations in average single scattering albedo and backscatter fraction among the sites studied. The errors increase when shorter-term variations in aerosol properties are considered; for monthly and hourly timescales, errors are expected to be greater than 8% and 15%, respectively, approximately one-third of the time. Systematic relationships exist between various aerosol optical properties [σ_{ap}, ω_o, b, $\Delta F/\delta$, and Ångström exponent ($å$)] and the amount of aerosol present (measured by σ_{sp}) that are qualitatively similar but quantitatively different among the four stations. These types of systematic relationships and the regional and temporal variations in aerosol optical properties should be considered when using ''climatological'' averages.

1. Introduction

Atmospheric aerosols affect the earth's radiative balance in several respects; one of these is by directly scattering and absorbing incoming solar radiation. The perturbation of the earth's radiative balance resulting from the scattering and absorption caused by anthropogenic aerosols has been termed direct aerosol radiative forcing and has been estimated globally to be similar in magnitude but opposite in sign to global greenhouse gas forcing (Houghton et al. 1996). Relative to greenhouse gases, the shorter atmospheric lifetime of aerosols results in more localized effects and regional differences in aerosol properties. Due to spatial and temporal differences in aerosol properties, it is necessary to measure aerosol properties on a regional scale with at least daily temporal resolution to determine aerosol radiative forcing. Satellite platforms provide opportunities to map aerosol properties on regional to global scales (King et al. 1999); however, the determination of aerosol radiative forcing from satellites requires assumptions about the chemical, microphysical, and optical properties of the aerosols because satellites do not measure several important aerosol properties (Tanre et al. 1997). Therefore, uncertainties in satellite-retrieved parameters can result from variability in aerosol properties that are assumed to be constant in retrieval algorithms. Documenting the magnitude of the spatial and temporal variation in aerosol optical properties is the first step in determining their contribution to the uncertainty in parameters derived from remotely sensed data. In addition to assessing uncertainty in retrieval algorithms, the variability in aerosol optical properties is important for the development of climate models. Sensitivity studies can indicate how important different

Corresponding author address: David Delene, John D. Odegard School of Aerospace Studies, University of North Dakota, Grand Forks, ND 58202-9007.
E-mail: delene@umac.org

TABLE 1. Station location and time period used for this study.

Site location	Bondville, IL	Lamont, OK	Sable Island, NS	Barrow, AK
Station ID	BND	SGP	WSA	BRW
Latitude	+40.053	+36.605	+43.933	+71.323
Longitude	+088.372	+097.485	+060.007	+156.609
Elevation (m)	230	315	5	8
Start of measurements	19 Sep 1996	6 Apr 1997	23 Nov 1994	6 Oct 1997
End of measurements	26 Sep 2000	26 Sep 2000	15 Apr 2000	26 Sep 2000

parameters are for determining properties of interest such as aerosol radiative forcing. Systematic relationships among aerosol properties can be used to check for consistency among measured and modeled climatologies. Also, systematic relationships can be used in model parameterization to reduce uncertainties resulting from insufficient knowledge of aerosol properties.

The objectives of this paper are to 1) summarize aerosol optical measurements made over several years at four North American surface monitoring stations in a manner useful to scientists doing aerosol remote sensing and modeling studies; 2) document regional variability in surface aerosol optical properties; 3) investigate seasonal, weekly, and daily variability of aerosol optical properties; and 4) document systematic relationships among aerosol optical properties. To accomplish these objectives, data from the National Oceanic and Atmospheric Administration's (NOAA) long-term surface aerosol monitoring network are analyzed. The dataset has been manually edited and has passed a recently developed quality assurance procedure. Aerosol optical properties measured at the surface may be different aloft; however, Sheridan and Ogren (1999) concluded that near-surface measurements of aerosol optical properties could, under some conditions, adequately represent the portion of the lower column that dominates the radiative effects. The Sheridan and Ogren (1999) study only applied to near-surface results, as the minimum altitude in the aircraft profiles was 50–300m AGL. Current research is studying the conditions under which surface measurements are representative of column aerosol optical properties.

2. Experimental methods

The NOAA Climate Monitoring and Diagnostics Laboratory began monitoring aerosols in the mid-1970s with baseline stations at Barrow, Alaska (BRW); Mauna Loa, Hawaii; American Samoa, and the South Pole. Since 1992, NOAA has been expanding its aerosol measurement program to include regional monitoring stations at Bondville, Illinois (BND); Lamont, Oklahoma (SGP); and Sable Island, Nova Scotia (WSA). These measurements are designed to characterize means, variabilities, and trends of climate forcing properties and to understand the factors that control these properties (Ogren 1995; Sheridan et al. 1998). In October of 1997, the aerosol instrumentation and sampling methodology were upgraded at BRW to match the three regional stations. To avoid possible interpretation problems we only analyze measurements made with the newer instrumentation [TSI 3563 nephelometer and radiance research particle soot absorption photometer (PSAP)] and sampling methodology. Table 1 gives the location of each station and the time periods covered by this study. Note that the time periods denoted in Table 1 contain some large (weeks to months) gaps due to instrument problems or station maintenance.

BND is an anthropogenically influenced continental station located at the Illinois State Water Survey's Bondville Environmental and Atmospheric Research site. The site is located 6.5 km south of Bondville, 16 km west of Champaign–Urbana (population 100 000), and is surrounded by corn and soybean fields. The SGP station is part of the Department of Energy, Southern Great Plains Cloud and Radiation Testbed (CART) site. The site is distant from any large urban areas so atmospheric aerosols at the site can be interpreted as representative of mixed regional aerosols; however, large point sources (oil refineries and power plants) may impact the site from time to time. Sheridan et al. (2001) recently summarized four years of microphysical and optical aerosol measurements made at the SGP site. WSA is an anthropogenically influenced marine station located on a small (41 km) island that is ~290 km southeast of Halifax, Nova Scotia. The BRW station is located 530 km north of the Arctic Circle on the Arctic Coast and is adjacent to the Department of Energy's North Slope of Alaska station. Due to their marine locations, BRW and WSA have major contribution to their aerosol optical properties from sea-salt particles.

Each monitoring site has a temperature-controlled building where the aerosol instruments and data acquisition system are housed. To minimize local contamination, aerosol samples are obtained from the top of an intake stack (~21.6-cm inner diameter) at a height of ~10 m above ground level. The intake stack has a rain cap and stainless steel screen to prevent water, birds, and insects from entering the sampling system. Airflow through the inlet stack is ~1000 L min^{-1} and is divided into two separate flows; these are a sample flow of ~150 L min^{-1} and a sheath flow of ~850 L min^{-1}. The sample flow is taken from the center of the stack tube and directed through a smaller stainless steel tube (~4.45-cm inside diameter), where the sample air is gently heated when necessary to achieve a relative humidity below

40%. The sample flow then enters a flow splitter where it is passed into five sampling lines (~30 L min^{-1} and 1.6-cm inside diameter). A switched impactor system is used to enable measurements of submicrometer and ''total'' [particle diameter (D_p) less than 10 μm] aerosol properties. A 10-μm aerodynamic diameter cutpoint impactor is always in-line and every 5–6 min a ball valve is opened or closed to switch the flow through or around a 1-μm aerodynamic diameter cutpoint impactor. Hence, alternating 10-μm ($D_p < 10$ μm) and 1-μm ($D_p < 1$ μm) size cut measurements are obtained. Sheridan et al. (2001) presents a more detailed description, including a system flow diagram, of the SGP system.

The aerosol optical properties measured at each station consist of aerosol light absorption coefficient (σ_{ap}), light scattering coefficient (σ_{sp}), and hemispheric backscattering coefficient (σ_{bsp}) made over the two size ranges. Unless otherwise noted, all aerosol measurements discussed here are for $D_p < 10$ μm, 550-nm wavelength, and at a relative humidity of 40% or less. The main reason for maintaining the relative humidity below 40% is so changes in measured aerosol properties can be attributed to changes in the amount or nature of aerosol particles and not the result of changes in ambient relative humidity. The σ_{ap} was measured using a filter-based light absorption photometer (radiance research model PSAP) that was calibrated to estimate suspended-state aerosol light absorption at 550 nm using an extinction cell and nephelometer (Bond et al. 1999). The σ_{sp} and σ_{bsp} were measured using a 3-wavelength (nominally 450, 550 and 700 nm) TSI Model 3563 nephelometer (Anderson et al. 1996; Anderson and Ogren 1998). The nephelometer operates by illuminating a fixed sample volume from the side and observing the amount of light that is scattered by particles and gas molecules in the direction of a photomultiplier tube. A particle filter is inserted periodically into the sample stream to measure scattering by gas molecules, which is subtracted from the total scattering in real time to determine scattering by aerosol particles. The TSI nephelometer measures σ_{sp} over an angular integration of 7°–170° and σ_{bsp} over an angular integration of 90°–170°. Besides the aerosol optical property measurements, aerosol chemistry and condensation nuclei (CN) measurements are also made at each site but are not discussed here. Quinn et al. (2000) has summarized results from filter measurements of submicron aerosol mass and the mass of major ionic components obtained at numerous locations including BND, WSA, and BRW. The SGP site was not included in Quinn's study because aerosol chemistry measurements were only recently added at SGP.

From the measurements made at each station, it is possible to determine the hemispheric backscatter fraction (b), Ångström exponent ($\mathring{a}$), aerosol single scattering albedo (ω_o), submicron scattering fraction (R_{sp}), and submicron absorption fraction (R_{ap}). These parameters are calculated as follows:

$$b = \frac{\sigma_{bsp}}{\sigma_{sp}}, \tag{1}$$

$$\mathring{a} = -\frac{\log(\sigma_{sp}^{550}/\sigma_{sp}^{700})}{\log(550/700)}, \tag{2}$$

$$\omega_o = \frac{\sigma_{sp}}{\sigma_{sp} + \sigma_{ap}}, \tag{3}$$

$$R_{sp} = \frac{\sigma_{sp}(D_p < 1\ \mu m)}{\sigma_{sp}(D_p < 10\ \mu m)}, \quad \text{and} \tag{4}$$

$$R_{ap} = \frac{\sigma_{ap}(D_p < 1\ \mu m)}{\sigma_{ap}(D_p < 10\ \mu m)}, \tag{5}$$

where b, ω_o, R_{sp}, and R_{ap} are referenced to 550-nm wavelength and the superscripts in (2) refer to wavelength. The measured parameters σ_{ap}, σ_{sp}, and σ_{bsp} reflect mainly the amount of aerosol present while the calculated parameters b, $\mathring{a}$, and ω_o reflect the nature of the aerosol particles. Aerosol properties that vary largely as a function of particle amount are termed ''extensive'' properties, while properties that relate to the nature of the aerosol are termed ''intensive'' properties (Ogren 1995).

Knowledge of the aerosol ω_o, b, and optical depth (δ) can be used to calculate the global mean, annually averaged, top of the atmosphere aerosol forcing (ΔF) from an optically thin, partially absorbing aerosol [Haywood and Shine 1995, Eq. (3)] and can be expressed as

$$\Delta F = -DS_o T_{at}^2 (1 - A_c)\omega_o \beta \delta \times \{(1 - R_s)^2 - (2R_s/\beta)[(1/\omega_o) - 1]\}, \tag{6}$$

where D is the fractional day length, S_o is the solar constant, T_{at} is the atmospheric transmission, A_c is the fractional cloud amount, R_s is the surface reflectance, and β is the average upscatter fraction (calculated from b). The aerosol forcing per unit optical depth is called aerosol forcing efficiency (Sheridan and Ogren 1999):

$$\frac{\Delta F}{\delta} = -DS_o T_{at}^2 (1 - A_c)\omega_o \beta \times \left\{(1 - R_s)^2 - \left(\frac{2R_s}{\beta}\right)\left[\left(\frac{1}{\omega_o}\right) - 1\right]\right\}. \tag{7}$$

By assuming no geographical variation of R_s and T_{at}, and no zenith angle dependence of β, and using the values $D = 0.5$, $S_o = 1370$ W m^{-2}, $T_{at} = 0.76$, $A_c = 0.6$, and $R_s = 0.15$ as suggested by Haywood and Shine (1995), Eq. (7) can be used to assess the intrinsic radiative forcing efficiency of aerosols. Wiscombe and Grams (1976) reported the relationship among β, b [calculated from nephelometer measurements with Eq. (1)], and the asymmetry parameter for the Henyey–Greenstein phase function and the current work uses a second-order curve fit to the points in their Fig. 3, which yields $\beta = 0.0817 + 1.8495b - 2.9682b^2$. The dependency of ω_o and β on relative humidity is ignored

in this analysis since the aerosol measurements were all made at a low controlled relative humidity (<40%). The relative humidity dependence of σ_{sp} and σ_{bsp} has been measured at BND (Koloutsou-Vakakis et al. 2001), WSA (McInnes et al. 1998) and SGP (Sheridan et al. 2001), which enables low relative humidity measurements to be adjusted to ambient relative humidity; however, the relative humidity dependency of σ_{ap} is not currently known. Anderson et al. (1999) discuss the results that hydrating the aerosol to 80% relative humidity would have on ω_o and β, and calculate the associated uncertainty. Similar uncertainties are expected for the dataset discussed here.

3. Aerosol data

A computer data acquisition system records raw measurements from each aerosol instrument with 1-min time resolution and system status information with 0.5-h time resolution. At WSA and BRW, the computer system flags data as contaminated based on wind direction and CN concentration. This is done to eliminate contamination from known local sources so measurements can be regarded as regional in scope. No contamination algorithm is used to flag polluted data at BND or SGP since no known strong local sources are nearby. Data files are retrieved daily from field computers for processing and archiving. As part of an ongoing data quality control procedure, the station scientist looks over data from the previous day to check for instrument or system problems. Also, the station scientist edits the data to remove data during the weekly station maintenance and invalid data resulting from instrumental or sampling problems. Weekly maintenance consists of changing the impactor films, a system leak check, and a nephelometer calibration check. By filling the nephelometer with particle-free gases of known scattering coefficients, the calibration is checked and a quantification of calibration drift and instrument noise is obtained as described by Anderson and Ogren (1998). Anderson et al. (1999) concluded that the nephelometer calibration uncertainty was ±7% and the PSAP calibration uncertainty was ±20%. Using the above measurement uncertainties, Anderson et al. (1999) estimated the total uncertainty for continental air masses (low relative humidity, nonsea-salt) to be 0.025 for b, 0.036 for ω_o, and 11% for $\Delta F/\delta$. Marine air masses (low relative humidity) uncertainties were estimated to be 0.041 for b, 0.014 for ω_o, and 21% for $\Delta F/\delta$.

The nephelometer scattering data were adjusted to conditions of standard temperature and pressure (STP) for comparison with the absorption measurements, which were referenced to STP. A nephelometer truncation correction was applied to the data following the method of Anderson and Ogren (1998). This corrects scattering measurements made over integration angles of ~7°–170° and ~90°–170° to the full 0°–180° and 90°–180° ranges, based on the measured $\mathring{a}$. The absorption measurements were corrected using the methods of Bond et al. (1999). This includes a spot size correction, an adjustment of the absorption measurement from 565-nm (PSAP wavelength) to 550-nm wavelength and a correction for filter-based scattering that is sensed as absorption by the PSAP. The nephelometer-measured scattering data were used to make the filter-based scattering correction; hence, absorption data were removed from the dataset during periods of invalid scattering measurements. Absorption data were also removed if the filter transmittance was below 0.5 and flagged as suspect if the filter transmittance was below 0.7. The suspect absorption data (filter transmittance from 0.5 to 0.7) were retained in the dataset discussed here.

Edited 1-min data files were created from the raw data files by excluding polluted data, applying manual edits, and making data corrections. The edited 1-min data files were averaged to create hourly averaged data files. Hourly averaged data with 50% or more valid measurements per hour and hourly averaged σ_{sp} (550 nm) above 1.0×10^{-6} m^{-1} (1.0 Mm^{-1}) comprise the data used for this study. The 1.0 Mm^{-1} limit is a noise threshold used to exclude data that have low signal to noise ratios due to very low aerosol concentration. The aerosol concentration is almost always above the noise threshold except during clean periods at BRW.

As part of a data quality assurance procedure, a computer algorithm was used to screen the hourly averaged data and flag anomalous data points. The algorithm performs checks for physically impossible data, such as $\omega_o > 1.0$, that can result from instrumental noise and are not necessarily removed from the dataset since doing so would bias the dataset. All anomalous data points are investigated and additional data editing is performed on the 1-min data if instrumental or sampling problems can be identified. The computer algorithm also performs a check to see if aerosol parameters are within the expected range. Parameters outside the expected range are manually investigated to determine if an instrumental problem caused the unusual value or if it resulted from an unusual aerosol event, such as smoke from a forest fire or a rapid change in aerosol concentration from a strong weather front passing the site. The same screening algorithm was used on all four stations; however, different ranges of expected values were used for each station. In addition to the screening algorithm, the quality assurance procedure also included the generation of time series and monthly statistical plots. Time series were checked for sudden jumps and discontinuities that may result from instrumental problems and monthly statistics were compared against previous years to check for anomalies. Yearly quality assurance reports, time series, and statistical plots are part of each station's quality assurance web page and are available on the NOAA Climate Monitoring and Diagnostics Laboratory (CMDL) web site (http://www.cmdl.noaa.gov).

TABLE 2. Mean and std dev of aerosol optical properties based on monthly averaged data. Numbers in parentheses denote the number of data points used in computing the statistics. See text for a definition of each parameter and Table 1 for the station location and measurement time period.

		BND	SGP	WSA	BRW
σ_{ap} (Mm^{-1})	$D_p < 10$	4.66 ± 2.27 (43)	2.46 ± 1.09 (29)	1.88 ± 0.73 (47)	0.39 ± 0.41 (25)
	$D_p < 1$	3.94 ± 1.80 (43)	2.08 ± 0.98 (37)	1.51 ± 0.66 (46)	0.36 ± 0.38 (25)
σ_{sp} (Mm^{-1})	$D_p < 10$	57.7 ± 17.7 (47)	46.9 ± 16.9 (34)	39.9 ± 7.2 (57)	9.76 ± 5.20 (25)
	$D_p < 1$	48.7 ± 14.7 (47)	37.5 ± 12.7 (40)	13.6 ± 6.17 (56)	6.17 ± 3.61 (25)
σ_{bsp} (Mm^{-1})	$D_p < 10$	6.68 ± 1.66 (47)	5.36 ± 1.52 (34)	4.50 ± 0.76 (51)	0.99 ± 0.48 (25)
	$D_p < 1$	5.59 ± 1.38 (47)	4.26 ± 1.20 (40)	1.75 ± 0.65 (50)	0.64 ± 0.34 (25)
ω_o	$D_p < 10$	0.924 ± 0.028 (43)	0.947 ± 0.025 (29)	0.956 ± 0.015 (47)	0.965 ± 0.023 (24)
	$D_p < 1$	0.924 ± 0.028 (43)	0.944 ± 0.025 (37)	0.897 ± 0.031 (45)	0.954 ± 0.028 (23)
B	$D_p < 10$	0.118 ± 0.009 (47)	0.117 ± 0.012 (34)	0.113 ± 0.006 (51)	0.105 ± 0.009 (24)
	$D_p < 1$	0.117 ± 0.009 (47)	0.115 ± 0.010 (40)	0.127 ± 0.011 (50)	0.106 ± 0.008 (23)
$\Delta F/\delta$ (W m^{-2})	$D_p < 10$	−23.8 ± 2.1 (43)	−25.4 ± 1.6 (29)	−25.3 ± 1.0 (44)	−25.2 ± 2.3 (24)
	$D_p < 1$	−23.6 ± 2.0 (43)	−25.0 ± 1.8 (37)	−22.6 ± 2.2 (42)	−24.5 ± 2.6 (23)
$\mathring{A}$	$D_p < 10$	2.03 ± 0.12 (47)	1.94 ± 0.21 (34)	0.77 ± 0.32 (57)	1.11 ± 0.39 (24)
	$D_p < 1$	2.37 ± 0.12 (47)	2.29 ± 0.15 (40)	2.32 ± 0.22 (56)	1.67 ± 0.36 (23)
R_{ap}	1/10	0.86 ± 0.11 (43)	0.87 ± 0.16 (29)	0.79 ± 0.16 (45)	0.87 ± 0.11 (24)
R_{sp}	1/10	0.85 ± 0.04 (47)	0.83 ± 0.06 (33)	0.34 ± 0.12 (56)	0.63 ± 0.14 (24)

4. Variability of aerosol properties

Hourly averaged aerosol data from BND, SGP, WSA, and BRW that have passed the data quality assurance procedure are analyzed in the following sections to investigate the variability in aerosol optical properties. Regional differences are analyzed by computing means and standard deviations of aerosol properties at each station. Yearly, weekly, and daily cycles are analyzed by examining statistical distributions for several important parameters. Systematic relationships among aerosol properties are documented and analyzed to determine their significance. During the 3–6 yr time period spanned by this study (Table 1) there are no obvious overall trends in the datasets except at SGP where an increase in σ_{ap}, and corresponding decrease in ω_o, was noted by Sheridan et al. (2001). Bodhaine and Dutton (1993) described a long-term decrease in arctic haze at BRW from 1982 to 1993, presumably from decreased anthropogenic emissions in Europe and the former Soviet Union.

a. Regional variability

Station means and standard deviations based on monthly averaged aerosol optical properties are given in Table 2. The monthly data used to compute the means and standard deviations were calculated from all valid hourly averaged data and only months with greater than 50% valid hourly data were included. The mean σ_{ap}, σ_{sp}, and σ_{bsp} values are highest at the anthropogenically influenced continental station of BND and lowest at BRW. The mean σ_{ap} at SGP is approximately half the mean σ_{ap} at BND while the mean σ_{sp} is only about 20% lower, which results in a lower mean ω_o at BND than at SGP. At WSA the mean ω_o ($D_p < 10$ μm) is larger than at BND and SGP, while the submicron ($D_p < 1$ μm) mean ω_o at WSA is the lowest among the four stations. The low submicron mean ω_o is probably the result of advection of pollution aerosols from the East Coast of the United States, while the high total mean ω_o reflects the importance of supermicron sea-salt aerosol. The mean b is highest at BND and lowest at BRW, while the mean $\Delta F/\delta$ is very similar at all the stations. The mean $\mathring{a}$ is lower at WSA and BRW than at the continental sites of BND and SGP due to the influence of large sea-salt aerosols at WSA and BRW. Submicron aerosols dominate the σ_{ap} ($R_{ap} \sim 0.85$) at all four stations and the σ_{sp} at BND, SGP, and BRW; in contrast, supermicron aerosols dominate the σ_{sp} ($R_{sp} = 0.32$) at WSA. Note that the R_{ap} is always larger than the R_{sp}, which indicates that submicron aerosols are more important in terms of absorption than scattering.

Table 3 is similar to Table 2 except station means and standard deviations are computed based on hourly averaged data instead of monthly averaged data. The calculated statistics exclude data with the σ_{sp} below 1.0 Mm^{-1} so noisy data at low concentrations do not make a major contribution to the standard deviations. This noise filter still allows noisy data to contribute to the calculation of R_{ap}; therefore, an additional restriction is used where hours with average σ_{ap} below 0.2 Mm^{-1} are excluded from the calculation of R_{ap}. Due to the timescale over which chemical measurements and satellite measurements are typically conducted, the monthly standard deviations are more appropriate when relating variations in measured aerosol optical properties to chemical measurements or chemical transport models, and the hourly standard deviations are more appropriate when relating variability to satellite observations. The standard deviations are higher for the hourly averaged data than monthly averaged data due to the increased variability of aerosol properties on the shorter timescale.

Since the corrections applied to the dataset discussed here have not been incorporated in many previous studies, comparisons with previous work should be made carefully. Anderson et al. (1999) quantify the magnitude

TABLE 3. Mean and std dev of aerosol optical properties based on hourly averaged data. The numbers in parentheses denote the number of data points used in computing the statistics. See text for a definition of each parameter and Table 1 for the station location and measurement time period.

		BND	SGP	WSA	BRW
σ_{ap} (Mm^{-1})	$D_p < 10$	4.62 ± 3.82 (26 070)	2.47 ± 2.71 (16 402)	1.89 ± 2.26 (26 248)	0.38 ± 0.54 (13 181)
	$D_p < 1$	3.91 ± 3.26 (26 081)	2.08 ± 2.63 (19 135)	1.52 ± 2.00 (25 896)	0.34 ± 0.49 (13 241)
σ_{sp} (Mm^{-1})	$D_p < 10$	57.0 ± 47.1 (30 627)	46.7 ± 42.8 (21 973)	40.7± 32.8 (32 599)	10.4 ± 11.1 (13 802)
	$D_p < 1$	48.2 ± 38.0 (30 604)	37.6 ± 33.7 (24 967)	14.1 ± 18.5 (32 200)	6.87 ± 6.08 (13 856)
σ_{bsp} (Mm^{-1})	$D_p < 10$	6.63 ± 4.50 (30 627)	5.34 ± 4.02 (21 962)	4.56 ± 3.32 (29 052)	1.06 ± 1.05 (13 699)
	$D_p < 1$	5.55 ± 3.71 (30 604)	4.27 ± 3.28 (24 954)	1.81 ± 1.98 (28 609)	0.66 ± 0.58 (13 761)
ω_o	$D_p < 10$	0.906 ± 0.067 (26 069)	0.932 ± 0.051 (16 402)	0.953 ± 0.038 (26 226)	0.959 ± 0.040 (11 902)
	$D_p < 1$	0.905 ± 0.071 (26 081)	0.928 ± 0.055 (19 134)	0.904 ± 0.066 (25 857)	0.949 ± 0.048 (11 286)
b	$D_p < 10$	0.130 ± 0.029 (30 627)	0.128 ± 0.028 (21 962)	0.118 ± 0.017 (29 045)	0.109 ± 0.019 (12 394)
	$D_p < 1$	0.128 ± 0.028 (30 604)	0.127 ± 0.027 (24 953)	0.133 ± 0.026 (28 570)	0.109 ± 0.019 (11 784)
$\delta F/\delta$ (W m^{-2})	$D_p < 10$	−23.5 ± 4.5 (26 069)	−25.4 ± 3.4 (16 392)	−25.6 ± 2.6 (23,728)	−25.1 ± 3.8 (11 869)
	$D_p < 1$	−23.1 ± 4.7 (26 081)	−24.9 ± 3.5 (19 121)	−23.4 ± 4.8 (23 308)	−24.4 ± 4.2 (11 263)
$\mathring{a}$	$D_p < 10$	2.03 ± 0.31 (30 627)	1.90 ± 0.46 (21 962)	0.83 ± 0.57 (32 593)	1.20 ± 0.56 (12 496)
	$D_p < 1$	2.39 ± 0.25 (30 604)	2.26 ± 0.38 (24 956)	2.29 ± 0.46 (32 155)	1.70 ± 0.50 (11 858)
*R_{ap}	1/10	0.87 ± 0.41 (25 488)	0.90 ± 0.39 (15 084)	0.77 ± 0.35 (23 461)	0.89 ± 0.22 (6523)
R_{sp}	1/10	0.85 ± 0.09 (30 568)	0.83 ± 0.11 (21 179)	0.36 ± 0.19 (31 814)	0.66 ± 0.18 (12 404)

* Data with hourly averaged σ_{ap} values below 0.2 Mm^{-1} are excluded from the dataset for this calculation.

of these corrections and present uncertainty estimates for various parameters based on air mass types. The range of submicron ω_o (0.886–0.974), b (0.106–0.139), and $\Delta F/\delta$ (−26 to −23 W m^{-2}) measurements during a 2 month campaign at a Pacific coastal station at Cheeka Peak, Washington (Anderson et al. 1999) compare well with the range of mean values among the four stations presented in Table 2. Note the $\Delta F/\delta$ range was adjusted from the range presented in Anderson et al. (1999) by using a surface reflectance 0.15 (assumed here for the calculation of $\Delta F/\delta$) instead of 0.07, which is more appropriate over the ocean.

b. Temporal variability

Monthly statistical distributions of aerosol properties based on all valid hourly average data from the period of study (Table 1) were analyzed for yearly cycles (Figs. 1–3). The statistical distributions are represented as box-whisker plots where the whiskers denote the 5 and 95 percentiles, the bottom and top of the box denote the 25 and 75 percentiles, and the horizontal line within the box denotes the 50 percentile. The 50 percentiles (median values) are typically different than the mean values given in Table 3 because the distributions are not normally distributed. The *y*-axis range in each plot varies from station to station so cycles at each site can be clearly identified. The last box-whisker in each plot gives the statistics for the entire study period and a horizontal line is used to denote the median value for entire study period so deviations above and below the median value can be easily identified.

Figure 1 shows that at BND, SGP, and WSA the σ_{ap} is highest in late summer and early fall, while the σ_{sp} is highest in midsummer. The σ_{ap} and σ_{sp} at BRW are highest in winter and very low during the summer. The σ_{ap} 5 percentile at BRW during the summer is below zero due to instrument noise at these low concentrations. The winter maximum in σ_{ap} and σ_{sp} at BRW corresponds to a winter maximum in submicron sulfate and sea-salt aerosol mass concentration (Quinn et al. 2000) and is indicative of arctic haze. Also, the higher σ_{sp} during the summer at BND and WSA corresponds with a summer maximum in submicron sulfate aerosol mass concentration (Quinn et al. 2000).

Figure 2 shows the monthly statistical distributions of $\mathring{a}$ and R_{sp} at the four stations. Strong seasonal cycles are evident at the marine sites (BRW and WSA) and slight seasonal cycles at the continental sites (BND and SGP). The similar seasonal cycles in $\mathring{a}$ and R_{sp} are indicative of the relationship of both parameters to the aerosol size distribution. The relative amount of sea-salt aerosol controls the seasonal cycles in $\mathring{a}$ and R_{sp} at BRW and WSA because it is the dominant marine supermicron aerosol (McInnes et al. 1997). Seasonal changes in $\mathring{a}$ and R_{sp} at BRW are probably controlled by seasonal changes in atmospheric flow patterns (Harris and Kahl 1994) and the amount of sea-ice cover.

The phase difference between the σ_{ap} and σ_{sp} cycles (Fig. 1) results in an autumn decrease in ω_o at BND and to a lesser extent at SGP (Fig. 3). The autumn decrease in ω_o at BND is persistent throughout mid-September to late October each year and may be related to agricultural harvesting activities. Large decreases in ω_o have been noted at BND when farmers are harvesting fields next to the station but the exact source of the absorbing aerosols is unknown. It may be due to the use of diesel farm tractors and trucks but is probably not caused by the mechanical production of large aerosols since $\mathring{a}$ and R_{sp} do not increase during this time period (Fig. 2). Also, there is no widespread crop or field burning near BND during this time period.

Figure 3 also shows seasonal variability in ω_o at WSA

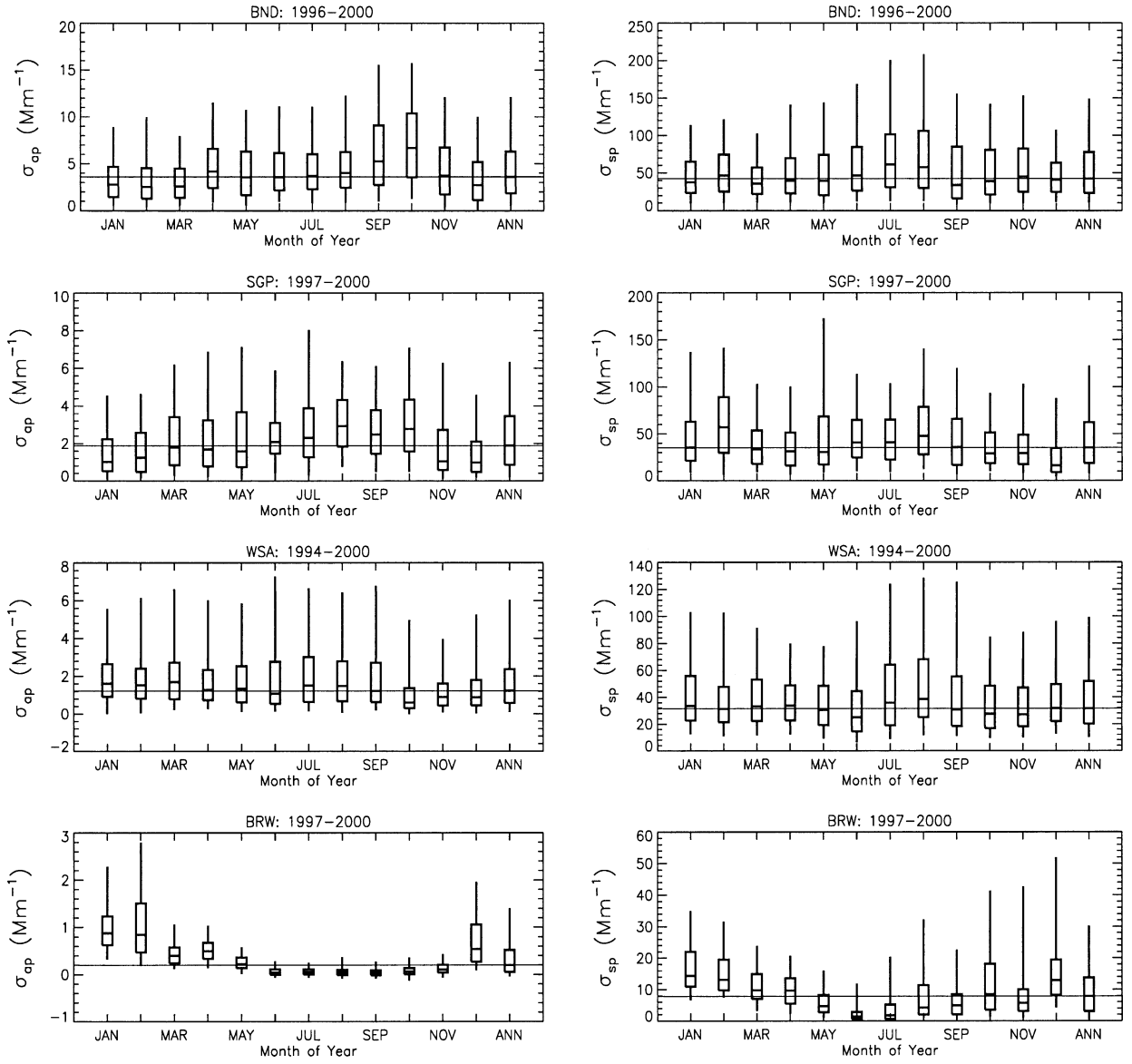

FIG. 1. Yearly cycle of absorption coefficient (σ_{ap}) and scattering coefficient (σ_{sp}) at BND, SGP, WSA, and BRW. The box and whiskers denote the 5, 25, 50, 75, and 95 percentiles. The statistics are based on the hourly averaged data for all valid measurements obtained during the study period denoted in Table 1. The *x* axis denotes the month of the year, with the last box-and-whisker denoting the percentile for the study period. The horizontal line denotes the median value for the entire study period.

and a strong seasonal cycle in ω_o at BRW. This strong seasonal cycle results in BRW having the lowest February median ω_o among the four stations while having the highest overall median ω_o. The high ω_o during the summer at BRW is expected of aerosols dominated by sea-salt particles as suggested by the low $\mathring{a}$ and R_{sp} seen in Fig. 2. In addition to the strong seasonal cycle in ω_o, BRW also has a strong seasonal cycle in *b* (Fig. 3). At BND, SGP, and WSA, less pronounced seasonal cycles in *b* are evident with low *b* occurring in summer instead of winter, as is the case at BRW.

Figure 4 shows daily statistical distributions of ω_o and *b* at the four sites. Daily cycles in ω_o and *b* are evident at BND and to a lesser extent at SGP, but not at WSA or BRW. The strong daily cycles at BND and SGP are clearly evident in all the percentiles of the distribution and result from similar daily cycles in σ_{ap} and σ_{sp}. The ω_o at BND and SGP is highest near local noon (1800 UTC), and the variability in the distribution is smaller near noon, especially at BND. The daily cycles in aerosol optical properties were also investigated by grouping the data by season and by month. Similar daily cycles (BND and SGP) or lack of daily cycles (WSA and BRW) were observed during each season and month as during the complete period (Fig. 4).

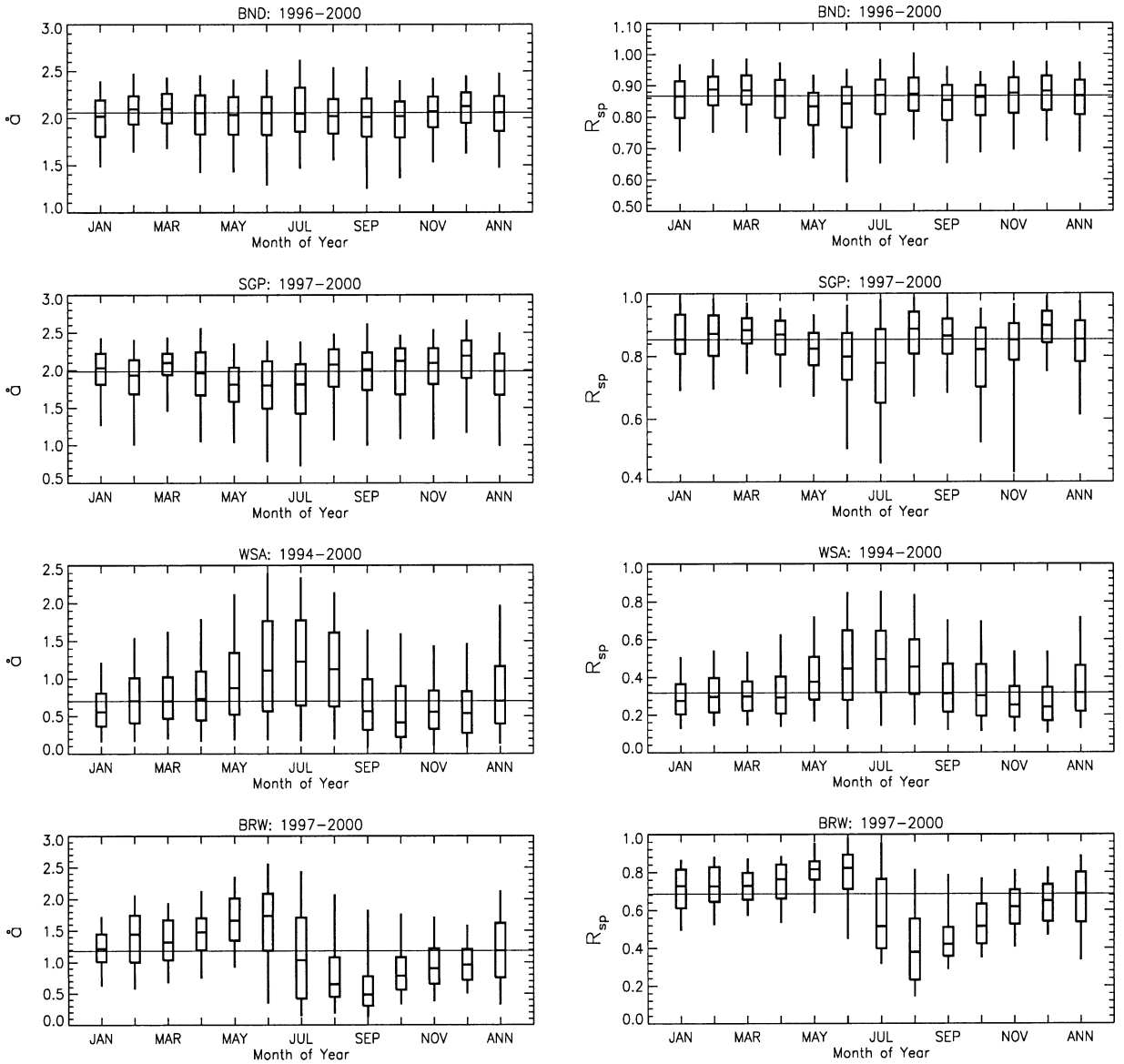

FIG. 2. Yearly cycle of Ångström exponent ($å$) and submicron scattering fraction (R_{sp}) at BND, SGP, WSA, and BRW. Plots are based on the same dataset and format as Fig. 1.

Figure 5 shows the day of the week statistical distributions of ω_o and b at the four sites. There is a weekly cycle in ω_o present at BND as is evident by the median ω_o changing from ~0.93 on Sunday to ~0.91 on Wednesday and the 5 and 75 percentiles both being higher on Sunday than during midweek. Also, SGP and BRW show some evidence of a weekly cycle with the Sunday statistics being different than midweek. BND and SGP show a slight (±0.02) variability in b, while no significant variability is present at WSA or BRW. Besides looking at the complete dataset, daily cycles were also investigated by grouping the data by season and by month of the year. The same weekly cycles or lack of weekly cycles were observed during each season and month as during the complete period.

c. Radiative forcing efficiency

To understand the importance of the yearly, daily, and weekly variations in ω_o and b to calculations of aerosol forcing, the $\Delta F/\delta$ is calculated as described earlier (Eq. 7) using the same assumed constants for all stations. The $\Delta F/\delta$ is nothing more than a zero-order estimate of radiative flux changes due to many simplifying assumptions (for example, neglect of the spectral dependence of aerosol and atmospheric optical properties, here studied only at 550 nm; neglect of changes in surface albedo, assumed here to be 0.15, despite obvious annual cycles in snow cover; and a low relative humidity, here 40% or less). It is important to note that the $\Delta F/\delta$ is for the top of the atmosphere and does not apply to radiative forcing at the

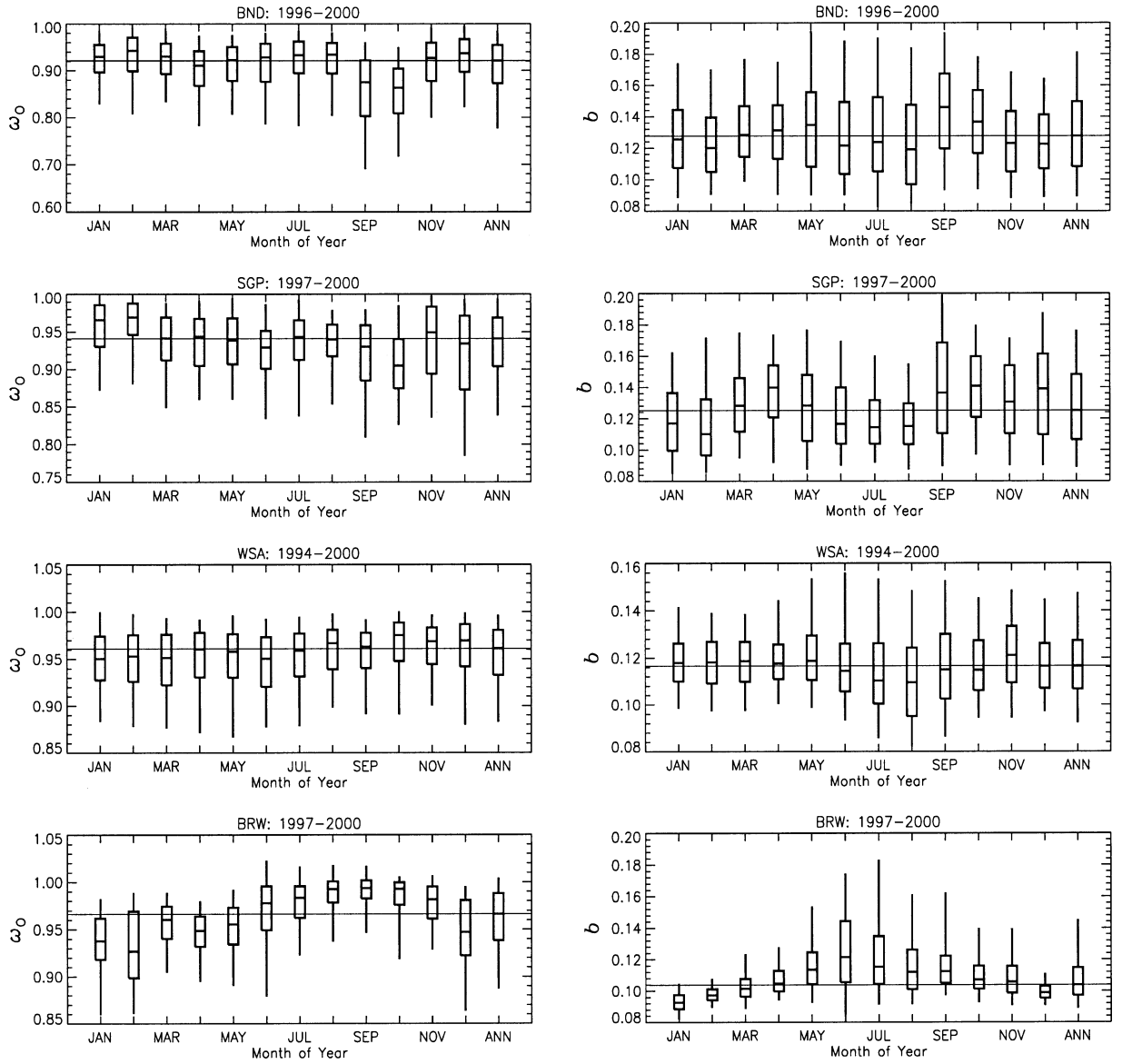

FIG. 3. Yearly cycles of aerosol single scattering albedo (ω_o) and hemispheric backscatter fraction (b) at BND, SGP, WSA, and BRW. Plots are based on the same dataset and format as Fig. 1.

surface. Despite these limitations, the $\Delta F/\delta$ is valuable in that it allows us to assess how variations in ω_o and b propagate into variations in direct climate forcing. An increase in ω_o or b will increase the magnitude of the $\Delta F/\delta$; therefore, when changes in ω_o and b are correlated they work together to change the $\Delta F/\delta$, and when they are anticorrelated they will offset each other so that the $\Delta F/\delta$ does not change very much.

Figure 6 shows the frequency distribution and monthly statistics of $\Delta F/\delta$ at BND, SGP, WSA, and BRW. The frequency distributions are similar among the four stations with WSA having a narrower distribution than the other stations. The autumn decrease in ω_o at BND is partially offset by an increase in b, which decreases the magnitude of the autumn anomaly in $\Delta F/\delta$. The less substantial autumn anomaly in ω_o at SGP is totally offset by an increase in b, which results in autumn distributions of $\Delta F/\delta$ similar to other times of the year. WSA shows very little monthly variation, while the strongly correlated seasonal cycles in ω_o and b at BRW combine to give a strong seasonal cycle in $\Delta F/\delta$.

Figure 7 shows the daily and weekly statistical distributions of $\Delta F/\delta$ at the four stations. The magnitude of the median $\Delta F/\delta$ difference between 0300–0400 UTC and 1800–1900 UTC at BND is $\sim$2 W m^{-2}. The Mann–Whitney u-test (similar to the Student's t-test except it does not require a normal distribution) indicates that at BND the 0300–0400 UTC $\Delta F/\delta$ mean is significantly ($<$0.001 significance level) different than the 1800–1900 UTC $\Delta F/\delta$ mean. At SGP there is a smaller

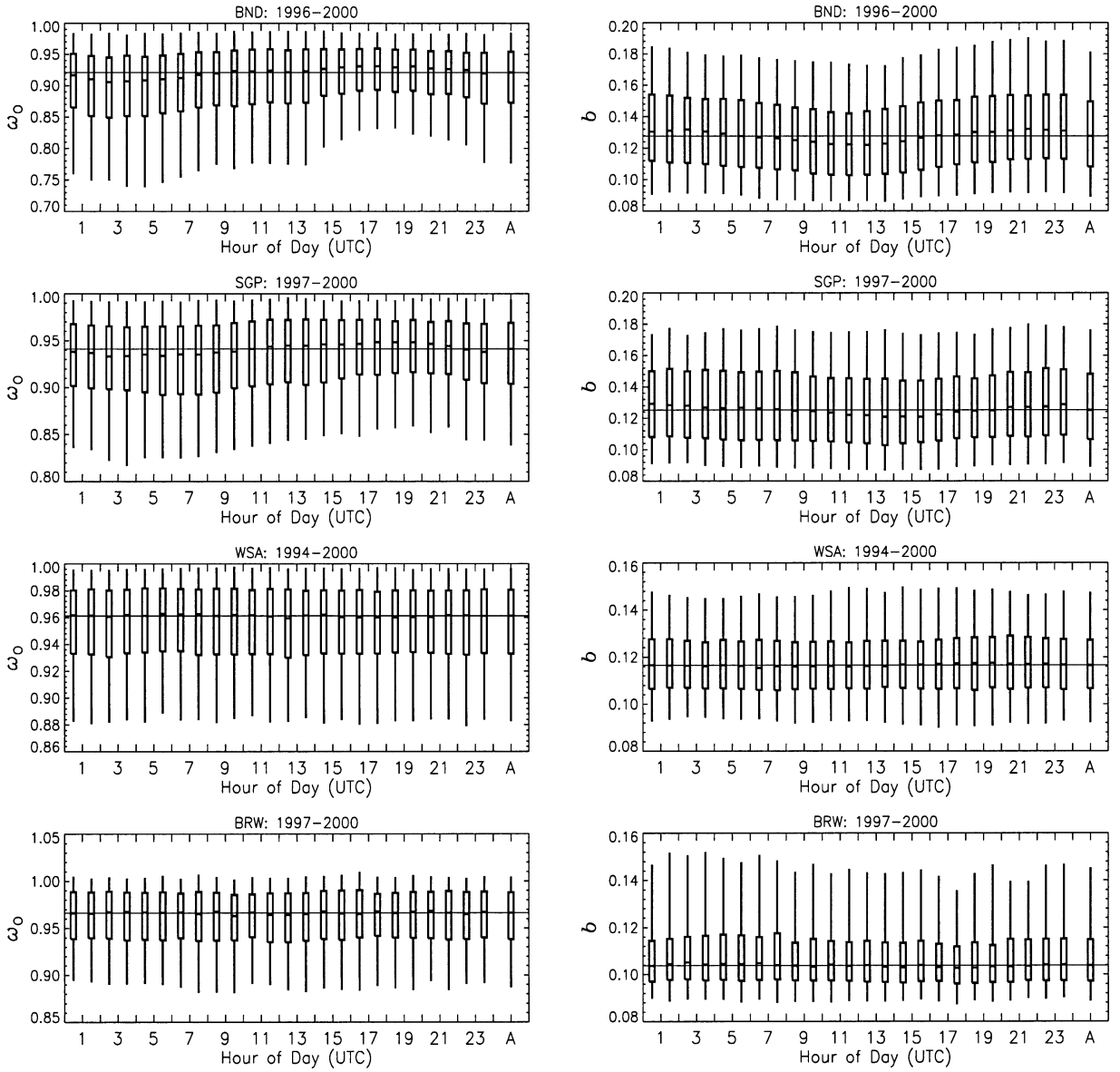

FIG. 4. Daily cycle in aerosol single scattering albedo (ω_o) and hemispheric backscatter fraction (b) at BND, SGP, WSA, and BRW. Plots are based on the same dataset and format as Fig. 1. Local standard time noon is 1800 UTC at BND and SGP, 1600 UTC at WSA, and 2100 UTC at BRW.

daily cycle with no daily cycles present at WSA or BRW. The stronger daily cycle at BND and lack of daily cycles at the more remote sites indicates that the proximity to source regions, such as urban centers, may be responsible for the daily variability in $\Delta F/\delta$. At all four stations, the $\Delta F/\delta$ mean is significantly (<0.001 significance level) different between Sunday and Wednesday; however, the magnitude of the median difference between Sunday and Wednesday is small.

d. Systematic relationships among aerosol properties

Knowledge concerning systematic relationships among aerosol properties can be useful in reducing uncertainties in remotely sensed data because they can be used to make better assumptions about unknown aerosol properties. Remer and Kaufman (1998) illustrated the importance of using a dynamic model where aerosol properties vary with aerosol load for the inversion of remote sensing data. The reason for using a dynamic aerosol model is to represent systematic changes in one aerosol property as another property changes. Due to their importance and usefulness, systematic relationships among aerosol optical properties were investigated at the four surface sites. Figure 8 shows systematic relationships among low relative humidity ($<40\%$) aerosol optical properties (σ_{ap}, ω_o, b, and $\Delta F/\delta$) and the aerosol load (measured as σ_{sp} at 550-nm wavelength).

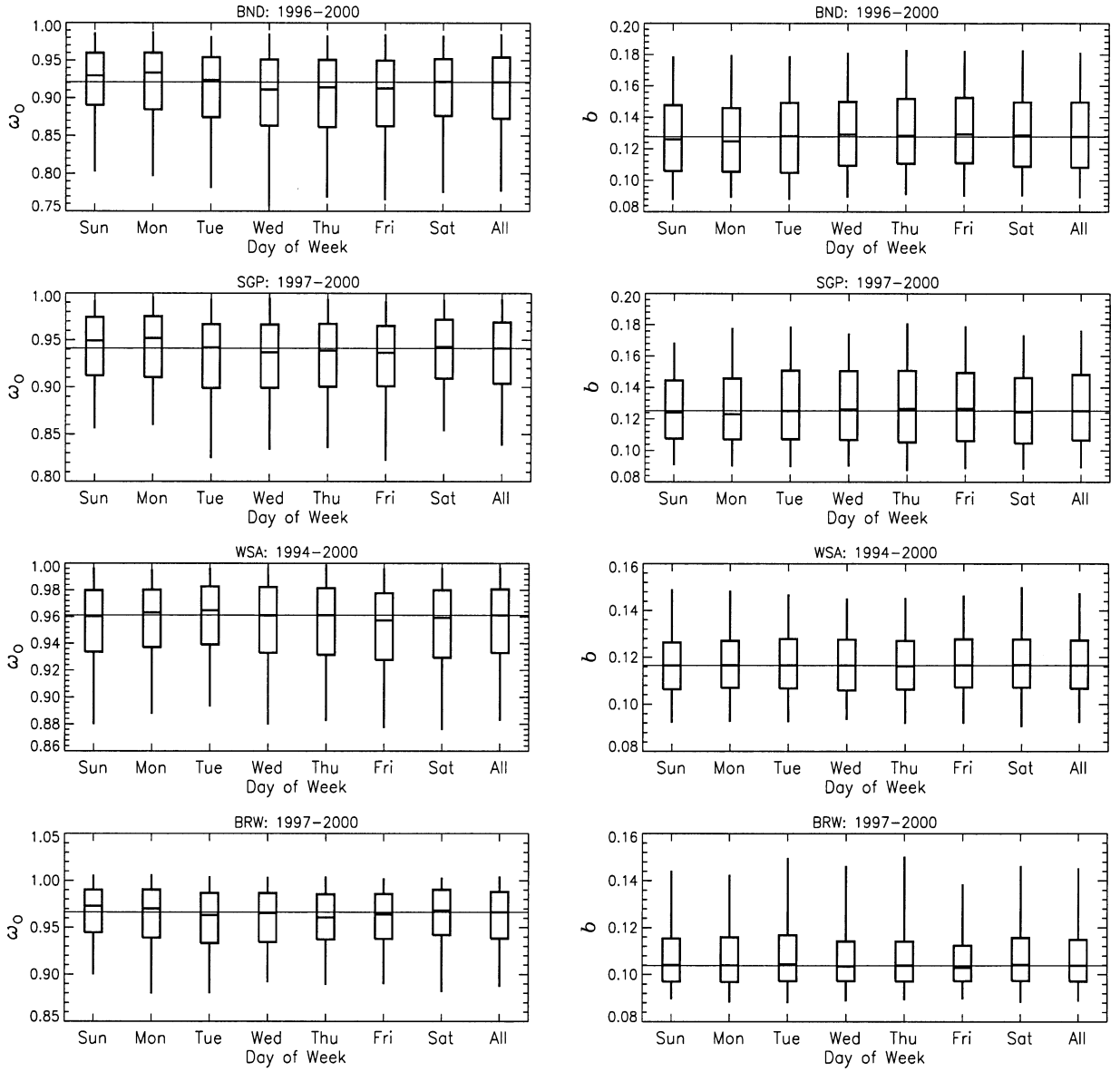

FIG. 5. Weekly cycle in aerosol single scattering albedo (ω_o) and hemispheric backscatter fraction (b) at BND, SGP, WSA, and BRW. Plots are based on the same dataset and format as Fig. 1.

The mean aerosol optical properties were calculated over σ_{sp} intervals of 10 Mm^{-1} with the maximum standard error for each station given in the text box. The standard errors are considerably smaller than the changes over 10-Mm^{-1} bins, which imply a high level of significance to the relationships. The σ_{ap} does not increase as rapidly as the σ_{sp}, which results in a systematic increase in ω_o as σ_{sp} increases at all four stations. All four stations also show a systematic decrease in b as σ_{sp} increases. In terms of $\Delta F/\delta$, the relationship between b and σ_{sp} acts to offset the relationship between ω_o and σ_{sp}. The b–σ_{sp} relationship results in a decrease in the magnitude of the $\Delta F/\delta$ as σ_{sp} increases, while the ω_o–σ_{sp} relationship results in an increase in the magnitude of the $\Delta F/\delta$ as σ_{sp} increases. For SGP and WSA, the b–σ_{sp} relationship is more important and results in a decrease in the magnitude of $\Delta F/\delta$ as σ_{sp} increases. For BND, the ω_o–σ_{sp} relationship is more important for σ_{sp} less than 40 Mm^{-1} and results in an increase in the magnitude of $\Delta F/\delta$ as σ_{sp} increases; however, above 40 Mm^{-1}, the b–σ_{sp} relationship is more important and results in a decrease in the magnitude of $\Delta F/\delta$ as σ_{sp} increases. Similarly, at BRW the relative importance of one relationship compared to the other determines how $\Delta F/\delta$ changes as σ_{sp} increases.

Figure 9 illustrates two systematic relationships, one between $\mathring{a}$ and σ_{sp} and the other between R_{sp} and $\mathring{a}$. The strong relationship between R_{sp} and $\mathring{a}$ indicates

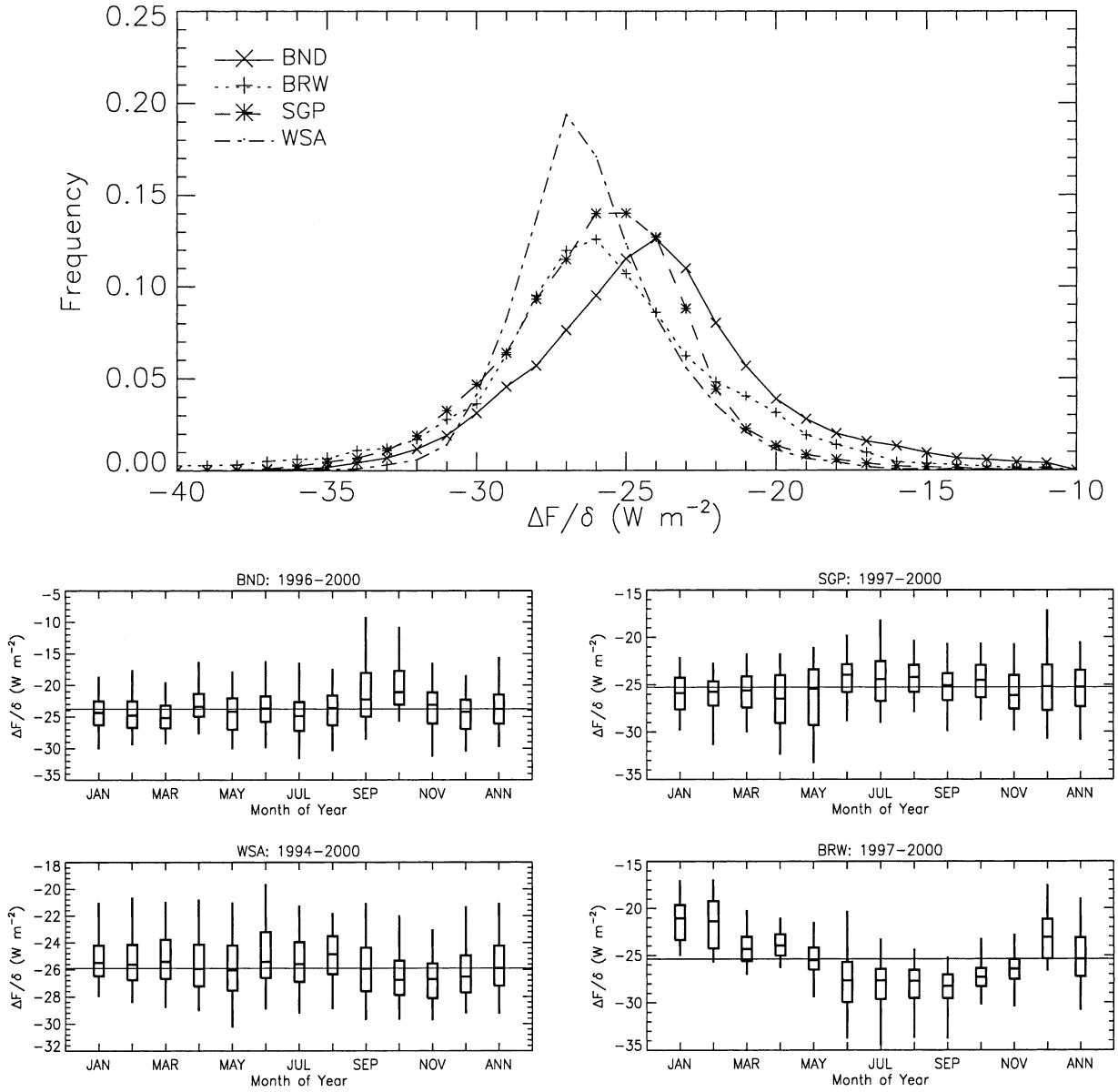

FIG. 6. Frequency distribution and yearly cycle in forcing efficiency ($\Delta F/\delta$) at BND, SGP, WSA, and BRW. Plots are based on the same dataset and format as Fig. 1.

that the $\mathring{a}$ is sensitive to changes in the relative amount of submicron scattering aerosol. At BND and SGP there is a drop in $\mathring{a}$ as σ_{sp} drops below 30 Mm^{-1}, while at WSA and BRW the $\mathring{a}$ increases as the σ_{sp} drops below 30 Mm^{-1}. Above 30 Mm^{-1} the stations show a fairly constant $\mathring{a}$ with increasing σ_{sp}; however, BND shows a downward trend at large (>60 Mm^{-1}) σ_{sp} suggestive of a slight increase in particle size. This systematic relationship suggests that during low aerosol concentration events, the continental sites (BND and SGP) have more relatively larger particles present, while the marine sites (WSA and BRW) have more relatively smaller particles present. The $\mathring{a}$–σ_{sp} relationship at BND and SGP (Fig. 9) is consistent with the relationship between the Ångström exponent and aerosol optical thickness (derived from sun–sky scanning spectral radiometer measurements) for the mid-Atlantic region of the eastern United States (Remer and Kaufman 1998). It is interesting to note that while the $\mathring{a}$–σ_{sp} relationship is different between SGP and WSA, the $\Delta F/\delta$–σ_{sp} relationship is very similar, which would suggest that $\Delta F/\delta$–σ_{sp} relationship is not influenced by changes in the submicron to total aerosol fraction but rather is influenced by changes in the submicron aerosol size distribution (b–σ_{sp} relationship) and the aerosol composition (ω_o–σ_{sp} relationship).

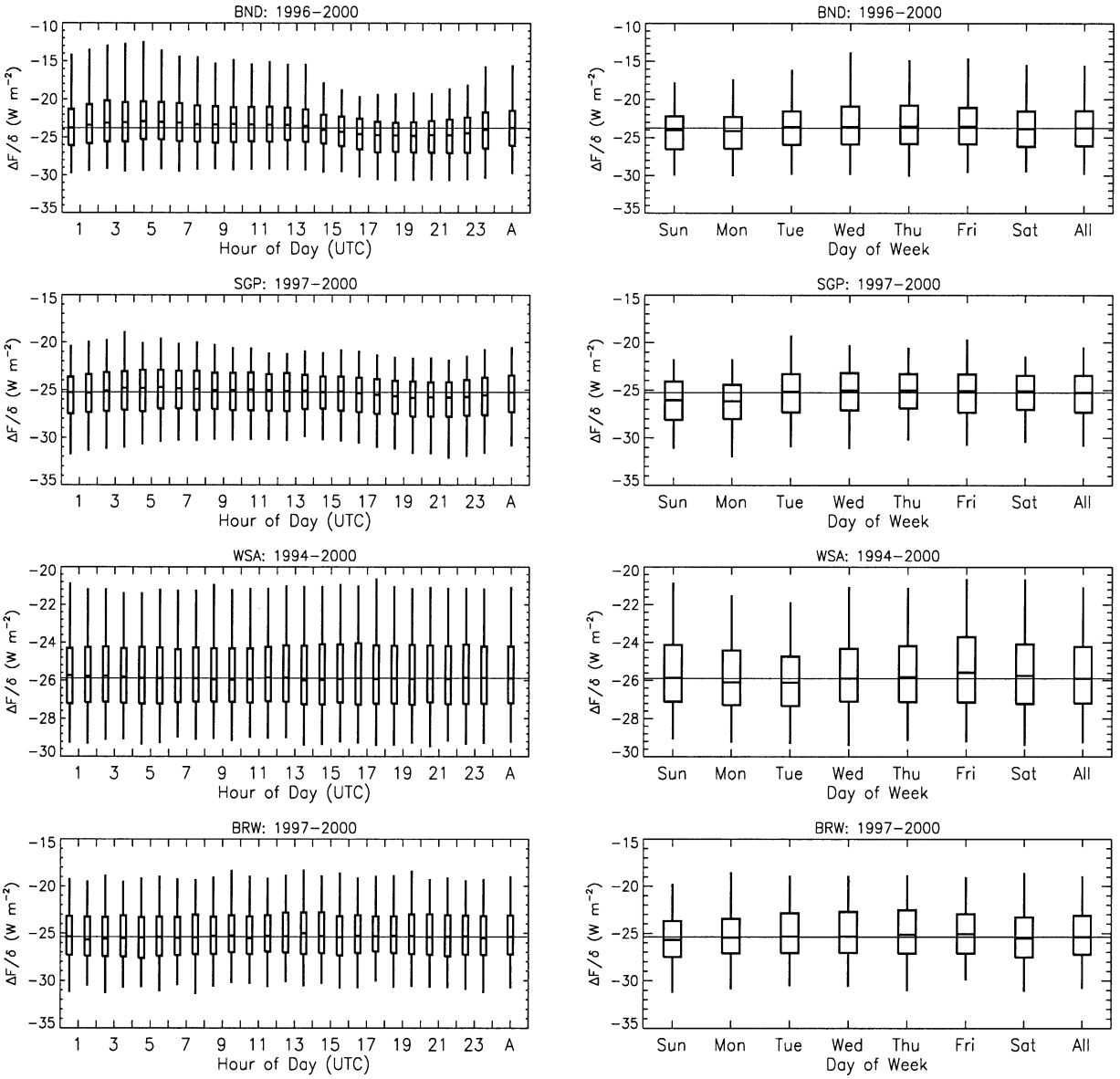

FIG. 7. Daily and weekly cycles in forcing efficiency ($\Delta F/\delta$) at BND, SGP, WSA, and BRW. Plots are based on the same dataset and format as Fig. 1. Local standard time noon is 1800 UTC at BND and SGP, 1600 UTC at WSA, and 2100 UTC at BRW.

5. Conclusions

Means and standard deviations of aerosol optical properties determined from several years of continuous surface measurements at four North American sites have been summarized. The mean σ_{ap} decreases by a factor of 10 and the σ_{sp} decreases by a factor of 5 between BND and BRW. The intensive aerosol properties of ω_o and b combine to give an approximate $\pm 4\%$ variability in mean radiative forcing efficiency ($\Delta F/\delta$) among the four sites. Yearly cycles in σ_{ap}, σ_{sp}, and σ_{bsp} are present at all four stations, along with yearly variations of ω_o and b, which combine to give less than 10% variation in median $\Delta F/\delta$. There are daily cycles in ω_o and b (Fig. 4) that result in a median variation in $\Delta F/\delta$ of $\pm 4\%$ at BND, a slight variation at SGP, and no significant variation at WSA and BRW. The small daily cycles in ω_o, b, and $\Delta F/\delta$ indicates that measurements at one time of the day can represent the annual average value with only a small uncertainty. This result is consistent with Kaufman et al. (2000) where they argue based on Aerosol Robotic Network (AERONET) data that single-time-of-day satellite aerosol measurements can represent annual average behavior at many sites to within 2% of data sampled every 15 min. It should be noted that the measurements presented here are surface-based while satellites see the entire column. Day of the week variations

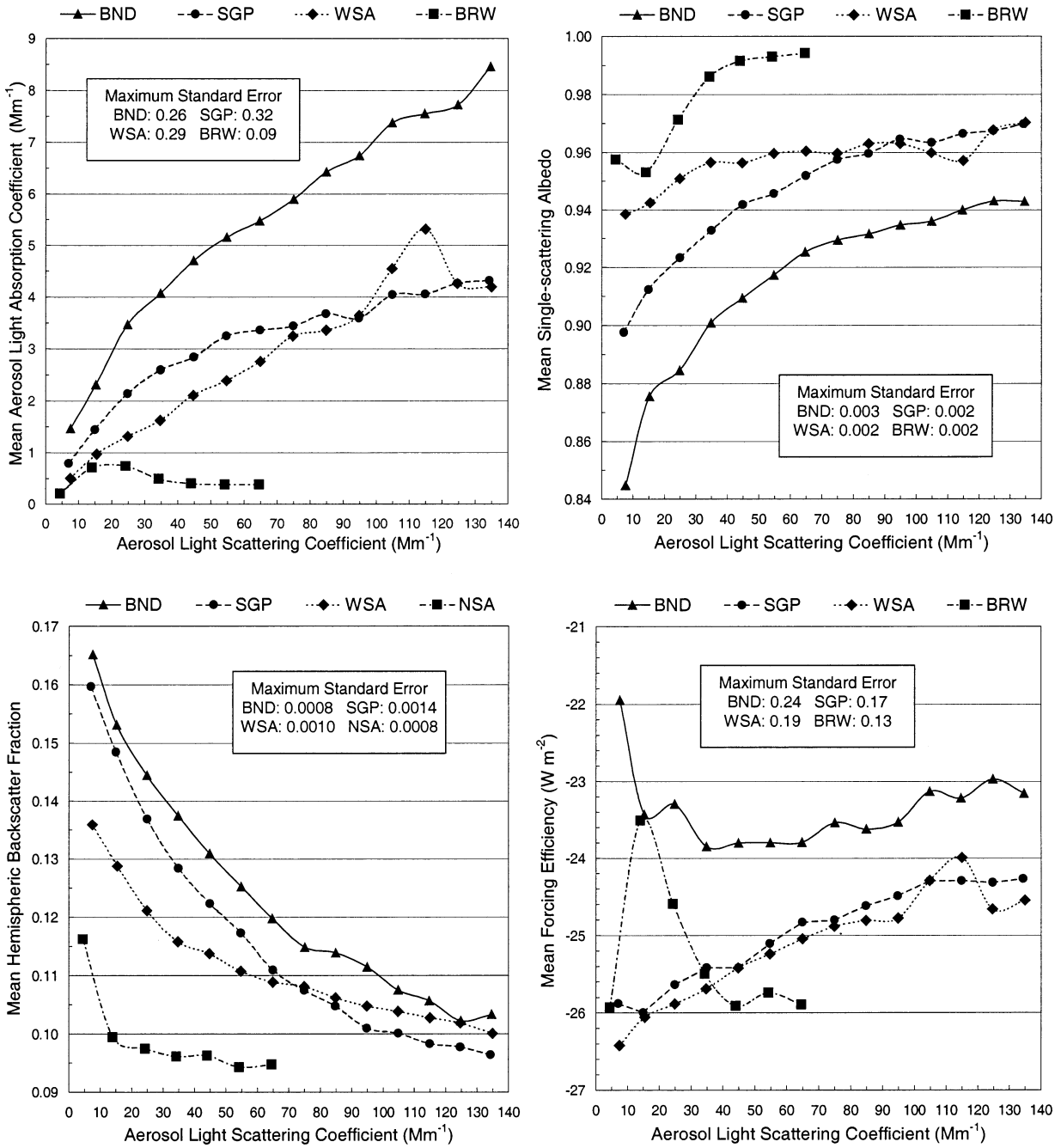

FIG. 8. Mean aerosol light absorption coefficient (σ_{sp}), single scattering albedo (ω_o), hemispheric backscatter fraction (b), and forcing efficiency ($\Delta F/\delta$) vs the aerosol light scattering coefficient (σ_{sp}) for BND, SGP, WSA, and BRW. Plots are based on all valid hourly averaged aerosol measurements (>50% 1-min data within the hour) made during the study period denoted in Table 1. The mean values were calculated over 10-Mm^{-1} σ_{sp} bins. The maximum standard error [sample std dev/square root (number of points)] at each station is given in the text boxes.

in mean $\Delta F/\delta$ were found at all four stations; however, the magnitude of the median variation in daily $\Delta F/\delta$ was small ($\sim\pm 1\%$).

Systematic relationships exist between various aerosol properties (σ_{ap}, ω_o, b, $\Delta F/\delta$, and $\mathring{a}$) and σ_{sp}, and also between $\mathring{a}$ and R_{sp}. These systematic relationships are qualitatively similar among the four stations; however, the quantitative relationships are different at each station, which is indicative of the occurrence of different aerosol types and size distributions at each station. Systematic relationships and the regional, yearly, weekly, and daily variations in optical properties can be used to

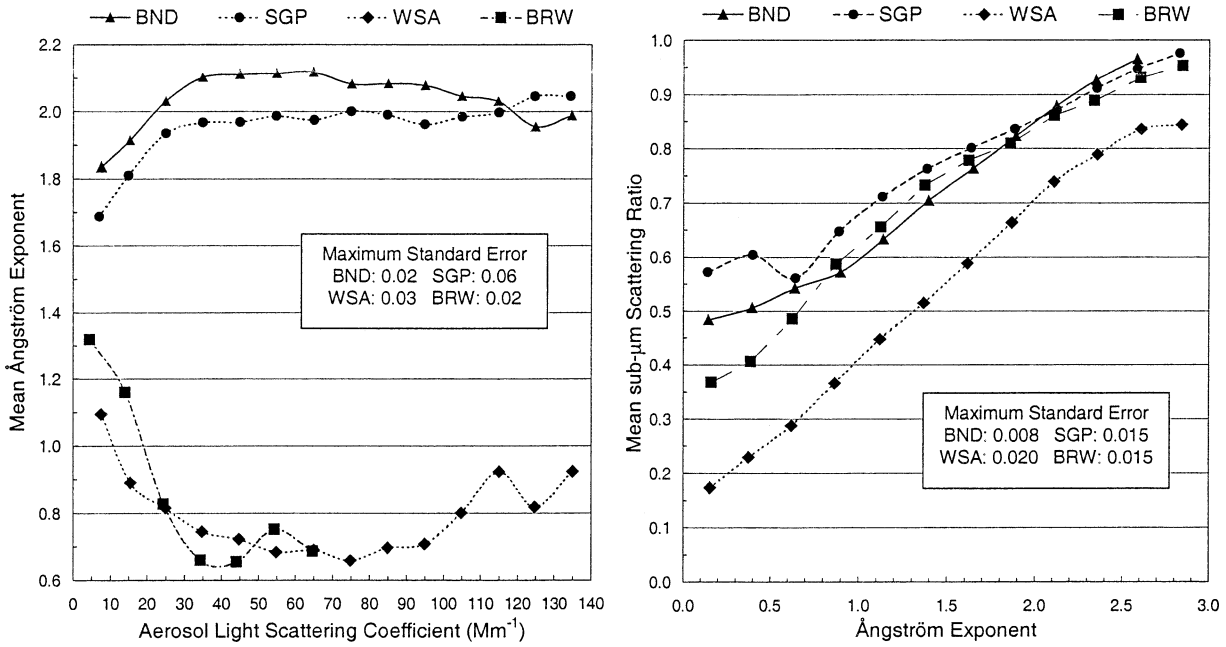

FIG. 9. Mean Ångström exponent ($\mathring{a}$) vs aerosol light scattering coefficient (σ_{sp}), and submicron scattering fraction (R_{sp}) vs Ångström exponent for BND, SGP, WSA, and BRW. Plots are based on all valid hourly averaged aerosol measurements (>50% 1-min data within the hour) made during the study period denoted in Table 1. The mean $\mathring{a}$ was calculated over 10-Mm^{-1} σ_{sp} bins and the mean R_{sp} was calculated over 0.25 Ångström exponent bins. The maximum standard error [sample std dev/square root (number of points)] at each station is given in the text boxes.

check for consistency between climatologies based either on observations or models. The existence of systematic changes in aerosol optical properties with changes in aerosol concentration indicate that care should be taken when using average values in algorithms to retrieve aerosol properties, such as optical depth, from satellite data. An algorithm that uses a static representation for aerosol optical properties will have a systematic bias in derived values.

The regional and seasonal variability among the four North American stations illustrates the necessity of quantifying aerosol properties on a regional scale over at least a 1-yr period. Based on the four North American stations analyzed in this study, the yearly, weekly, and daily cycles in intensive aerosol optical properties (ω_o and b) can result in uncertainties in radiative forcing calculations. Radiative transfer calculations that assume fixed aerosol properties can have errors of 1%–6% in the annual average forcing at the top of the atmosphere due to variations in average single scattering albedo and backscatter fraction among the sites studied. The errors increase when shorter-term variations in aerosol properties are considered; for monthly and hourly timescales, errors are expected to be greater than 8% and 15%, respectively, approximately one-third of the time. These uncertainties may further increase due to variation in relative humidity and the response of aerosol properties to relative humidity changes. The small variability in $\Delta F/\delta$, compared to the large variability in extensive aerosol properties (Fig. 1), indicates that only the extensive properties need to be characterized with high spatial resolution. Satellite measurements of aerosol optical depth combined with a select number of in situ measurements to determine regional intensive aerosol properties would seem to be able to determine aerosol forcing with a small amount of uncertainty.

Acknowledgments. We would like to thank Patrick Sheridan, Betsy Andrews, and three anonymous reviewers for their comments on this manuscript. We would like to acknowledge the contributions of the numerous people who fabricated, deployed, and supported the aerosol sampling system at the four monitoring sites. The NASA Global Aerosol Climatology Project provided data analysis support for this work. The Department of Energy ARM program funded the instruments and operation of the aerosol measurements at SGP. The ARM program also provided funding for new instruments used in the BRW upgrade. NOAA base funding provided for the operation of the BRW aerosol measurements and NOAA's Office of Global Programs funded the measurements at BND and WSA.

REFERENCES

Anderson, T. L., and J. A. Ogren, 1998: Determining aerosol radiative properties using the TSI 3563 integrating nephelometer. *Aerosol Sci. Technol.,* **29,** 57–69.

——, and Coauthors, 1996: Performance characteristics of a high-sensitivity, three-wavelength, total scatter/backscatter nephelometer. *J. Atmos. Oceanic Technol.,* **13,** 967–986.

——, D. S. Covert, J. D. Wheeler, J. M. Harris, K. D. Perry, B. E. Trost, D. J. Jaffe, and J. A. Ogren, 1999: Aerosol backscatter fraction and single scattering albedo: Measured values and uncertainties at a coastal station in the Pacific Northwest. *J. Geophys. Res.*, **104,** 26 793–26 807.

Bodhaine, B. A., and E. G. Dutton, 1993: A long-term decrease in arctic haze at Barrow, Alaska. *Geophys. Res. Lett.*, **20,** 947–950.

Bond, T. C., T. L. Anderson, and D. Campbell, 1999: Calibration and intercomparison of filter-based measurements of visible light absorption by aerosols. *Aerosol Sci. Technol.*, **30,** 582–600.

Harris, J. M., and J. D. W. Kahl, 1994: Analysis of 10-day isentropic flow patterns for Barrow, Alaska: 1985–1992. *J. Geophys. Res.*, **99,** 25 845–25 855.

Haywood, J. M., and K. P. Shine, 1995: The effect of anthropogenic sulfate and soot aerosol on the clear sky planetary radiation budge. *Geophys. Res. Lett.*, **22,** 603–606.

Houghton, J. T., L. G. Meira Filho, B. A. Callander, N. Harris, A. Kattenberg, and K. Maskel, Eds.,1996: *Climate Change 1995: The Science of Climate Change.* Cambridge University Press, 572 pp.

Kaufman, Y. J., B. N. Holben, D. Tanre, I. Slutsher, A. Smirnov, and T. F. Eck, 2000: Will aerosol measurements from Terra and Aqua polar orbiting satellites represent the daily aerosol abundance and properties? *Geophys. Res. Lett.*, **27,** 3861–3864.

King, M. D., Y. J. Kaufman, D. Tanre, and T. Nakajima, 1999: Remote sensing of tropospheric aerosols from space: Past, present, and future. *Bull. Amer. Meteor. Soc.*, **80,** 2229–2259.

Koloutsou-Vakakis, S., and Coauthors, 2001: Aerosol properties at a midlatitude Northern Hemisphere continental site. *J. Geophys. Res.*, **106,** 3019–3032.

McInnes, L. M., D. Covert, and B. Baker, 1997: The number of sea-salt, sulfate, and carbonaceous particles in the marine atmosphere. *Tellus*, **49B,** 300–313.

——, M. H. Bergin, and J. A. Ogren, 1998: Apportionment of light scattering and hygroscopic growth to aerosol composition. *Geophys. Res. Lett.*, **25,** 513–516.

Ogren, J. A., 1995: A systematic approach to in situ observations of aerosol properties. *Aerosol Forcing of Climate,* R. J. Charlson and J. Heintzenberg, Eds., John Wiley, 215–226.

Quinn, P. K., and Coauthors, 2000: Surface submicron aerosol chemical composition: What fraction is not sulfate? *J. Geophys. Res.*, **105,** 6785–6805.

Remer, L. A., and Y. J. Kaufman, 1998: Dynamic aerosol model: Urban/industrial aerosol. *J. Geophys. Res.*, **103,** 13 859–13 871.

Sheridan, P. J., and J. A. Ogren, 1999: Observations of the vertical and regional variability of aerosol optical properties over central and eastern North America. *J. Geophys. Res.*, **104,** 16 793–16 805.

——, J. Barnes, M. Bergin, M. Doorenbosch, W. Huang, A. Jefferson, J. Ogren, and J. Wendell, 1998: NOAA/Climate Monitoring and Diagnostics Laboratory Summary Report, 1996–1997. NOAA/CMDL Tech. Rep. 24, 166 pp.

——, D. J. Delene, and J. A. Ogren, 2001: Four years of continuous surface aerosol measurements from the Department of Energy's Atmospheric Radiation Measurement Program Southern Great Plains Cloud and Radiation Testbed site. *J. Geophys. Res.*, **106,** 20 735–20 747.

Tanre, D., Y. J. Kaufman, M. Herman, and S. Mattoo, 1997: Remote sensing of aerosol properties over oceans using the MODIS/EOS spectral radiances. *J. Geophys. Res.*, **102,** 16 971–16 988.

Wiscombe, W. J., and G. W. Grams, 1976: The backscattered fraction in two stream approximations. *J. Atmos. Sci.*, **33,** 2440–2451.